Mapping the susceptibility of rainfall and earthquake triggered landslides along China–Nepal highways

Article *in* Bulletin of Engineering Geology and the Environment · August 2019

DOI: 10.1007/s10064-019-01583-2

CITATIONS
8

READS
653

7 authors, including:

Kaushal Raj Gnyawali
University of British Columbia - Okanagan
18 PUBLICATIONS **144** CITATIONS
SEE PROFILE

Guojie Wang
Nanjing University of Information Science & Technology
93 PUBLICATIONS **1,891** CITATIONS
SEE PROFILE

Miao Lijuan
Nanjing University of Information Science & Technology
38 PUBLICATIONS **469** CITATIONS
SEE PROFILE

Ananta MS Pradhan
Water Resources Research and Development Centre
78 PUBLICATIONS **424** CITATIONS
SEE PROFILE

Bulletin of Engineering Geology and the Environment (2020) 79:587–601
https://doi.org/10.1007/s10064-019-01583-2

CASE HISTORY

Mapping the susceptibility of rainfall and earthquake triggered landslides along China–Nepal highways

Kaushal Raj Gnyawali[1,2] · Yonghong Zhang[1] · Guojie Wang[1] · Lijuan Miao[1,3] · Ananta Man Singh Pradhan[4] · Basanta Raj Adhikari[5,6] · Liming Xiao[7]

Received: 7 February 2019 / Accepted: 14 July 2019 / Published online: 12 August 2019

Abstract

The 2015 Gorkha earthquake (Mw = 7.8) caused significant earthquake triggered landslides (ETL) in a landscape that is heavily intervened by rainfall triggered landslides (RTL). China's Belt and Road Initiative plan to boost South-Asian regional trade and mobility through two key highway corridors, i.e. 1) Longmu–Rasuwa–Kathmandu (LRK) and 2) Nyalam–Tatopani–Kathmandu (NTK) route, that dissect the Himalayas through this geologically unstable region. To understand the spatial characteristics and susceptibility of these ETL and RTL, we delineate the landslides by means of time variant satellite imageries, assess their spatial distribution and model their susceptibilities along the highway slopes. We use a coupled frequency ratio (FR) – analytical hierarchy process (AHP) model by considering nine landslide determinants, e.g. geomorphic type (slope, aspect, curvature, elevation), hydrologic type (erosive potential of gullies, i.e. stream power index and distance to streams), normalized difference vegetation index, lithology and civil structure type (i.e. distance to roads). The results demonstrate that elevation and slope predominantly control both these landslide occurrences. The model predicts locations of ETL with higher accuracy than RTL. On comparison, NTK was safer with 133.5 km^2 of high RTL or ETL (or both) landslide susceptible areas, whereas LRK has 216.04 km^2. For mapping the extent of these landslides, we constricted it to the slope units of highways to reduce the computational effort, but this technique successfully achieved an acceptable threefold average model prediction rate of 82.75% in ETL and 77.9% in RTL. These landslide susceptibility maps and route comparisons would provide guidance towards further planning, monitoring, and implementing landslide risk mitigation measures for the governments.

Keywords Landslides susceptibility · Analytical hierarchy process · Gorkha earthquake · China · Nepal · Highways

Introduction

The 25 April 2015 Gorkha earthquake (Mw = 7.8) triggered over 20,000 landslides of various types in the mountainous terrains of Nepal and China covering an 87 km^2 area (Gnyawali and Adhikari 2017; Roback et al. 2018). The earthquake statistics suggest the deaths of 8964 people, 21956 injured and damage of about 10 billion USD (~50% of Nepal's nominal GDP) (Goda et al. 2015). These landslides blocked river valleys (Collins and Jibson 2015) and created huge dam-

✉ Yonghong Zhang
zyh@nuist.edu.cn

Kaushal Raj Gnyawali
gnyawalikr@hri.org.np

[1] School of Geographical Sciences, Nanjing University of Information Science and Technology (NUIST), Nanjing 210044, China

[2] Natural Hazards Section, Himalayan Risk Research Institute (HRI), Bhaktapur 44800, Nepal

[3] Department of Structural Development of Farms and Rural Areas, Leibniz Institute of Agricultural Development in Transition Economies (IAMO), 06120 Halle, Germany

[4] Department of Ocean Engineering, Pukyong National University, Busan, South Korea

[5] Institute for Disaster Management and Reconstruction, Sichuan University, Chengdu, China

[6] Department of Civil Engineering, Institute of Engineering, Tribhuvan University, Kathmandu, Nepal

[7] Department of Information and Communication, Nanjing University of Information Science and Technology (NUIST), Nanjing 210044, China

age along the road corridors (Hashash et al. 2015). This earthquake occurred in a landscape that is heavily intervened by rainfall triggered landslides. In August 2014, a large rock avalanche (~5 × 106 m3 volume) triggered by intense rainfall along the China–Nepal highway killed 155 people and destroyed 120 houses completely (Jaboyedoff et al. 2015). When the daily rainfall exceeds 144 mm, the risk of landslides on these Himalayan slopes is higher (Dahal and Hasegawa 2008). The China–Nepal Highway, an important part of China's Belt and Road Initiative (BRI) to improve regional trade and cooperation on a transcontinental scale (Rana and Karmacharya 2016), has to traverse these exceptional terrain conditions. This route is vital to improve the north–south connectivity for regional trade between China, Nepal, India and beyond (Beazley and Lassoie 2017; Rana and Karmacharya 2016) through a series of trans Himalayan corridors. This expanded transportation network will have to face an escalated risk of landsliding because of the interplay of these earthquake triggered (ETL) and rainfall triggered landslides (RTL).

Landslides create significant challenges in road construction, maintenance, and mobility in this region (Dongtao et al. 2004; Hearn and Shakya 2017). McAdoo et al. (2018) found that the occurrence probability of landslides on roadside slopes is multi-fold more intense than on normal slopes here. The damage and susceptibility assessment carried out shortly after the 2015 earthquake by (Xu et al. 2017) found about ~3 ETL per square km of land in these highway corridors. However, a comprehensive landslide susceptibility assessment requires data from both ETL and RTL landslides (Bai et al. 2013; Li et al. 2012; Tian et al. 2016).

Landslide susceptibility involves the spatial distribution and probability rating of the terrain units to produce landslides depending on the topography, geology, geotechnical properties, climate, vegetation, and anthropogenic factors (Fell et al. 2008; Guzzetti et al. 2005). The methods of landslide susceptibility assessment (LSA) can be classified into three basic types: knowledge-driven, data-driven and physically based methods (Corominas et al. 2013). Knowledge-driven methods exploit the expert-based weighting of different landslide related factors. Data-driven methods use statistical comparisons of factors that triggered past landslides and make quantitative predictions for current non-landslide-affected areas. Physically based models calculate slope stability based on geo-mechanical failure processes. LAS is now an established science with standard guidelines (Fell et al. 2008) and workflows for consistent presentation and meta-analysis (Lombardo and Mai 2018). The AHP (Saaty 1980) is a powerful data-driven tool for creating landslide susceptibility maps (Demir et al. 2013; Kayastha et al. 2013; Myronidis et al. 2016). Pairwise comparisons of individual controlling factors help to assign weight values to them (Saaty 1980; Saaty 2005; Saaty and Vargas 2001). Coupling the AHP with frequency ratio during pairwise comparison makes this method robust for landslide susceptibility assessment (Myronidis et al. 2016; Pradhan and Kim 2016). In LSA, during the model validation stage, repeated k-fold cross validation eliminates the peculiar random characteristics of a single data partition by using different subsets of the same data as training and validation sets and thus effectively using the entire dataset (Petschko et al. 2014). Using this technique, we can further determine the confidence interval associated with assigning mean susceptibility values to the terrain mapping units (Camilo et al. 2017).

Although comparative studies of ETL and RTL susceptibility for a few regions are available, (Bai et al. 2013; Goda et al. 2015; Li et al. 2012; Zhang et al. 2018), their integrated susceptibility assessments for highway corridors and route comparison has not been done before. Further, to save computational effort, on constricting the mapping and analysis region to the highway slope units, i.e. the slopes that can contribute landslide debris from or away from to the highway; can significant accuracy be achieved in these models? This is another question to be addressed. The 2015 Gorkha earthquake provided an unprecedented opportunity to assess both the ETL and RTL susceptibility of these vital highways in this seismic and hydro climatically active region.

In this study, we delineate, compare and model the susceptibility of ETL and RTL in the slope units of China Nepal highways (i.e. LRK and NTK). We perform weight analysis of each landslide determinants using a coupled frequency ratio-analytical hierarchy (FR-AHP) method and further compare the two routes for landslides susceptibility. We test the model accuracy using a threefold cross validation to assure our prediction results. The main difference between this study and previous research is a combined approach of susceptibility assessment to both ETL and RTL by constricting the computational region to the highway slope units and route comparison.

Study area and data

Study area

The study area is the China–Nepal highways that are an important part of China's Belt and Road Initiative (BRI). This comprises two arterial routes connecting Lhasa (the western transportation hub of China) in the Tibetan plateau to the Kathmandu valley (Nepal's capital city). They are the Longmu–Rasuwa–Kathmandu route (LRK) and the Nyalam–Tatopani–Kathmandu route (NTK), Fig. 1. Both routes cross the mighty Himalayan range, snaking their way between ravines and peaks.

This region has high seismic hazard (Mugnier et al. 2017) that accommodates continental convergence rate at 20 mm/yr. of the seismogenic Main Himalayan Thrust (Lavé and Avouac 2000). The inactive Main Central Thrust (MCT) crosses both the routes laterally. This region is also recognized for

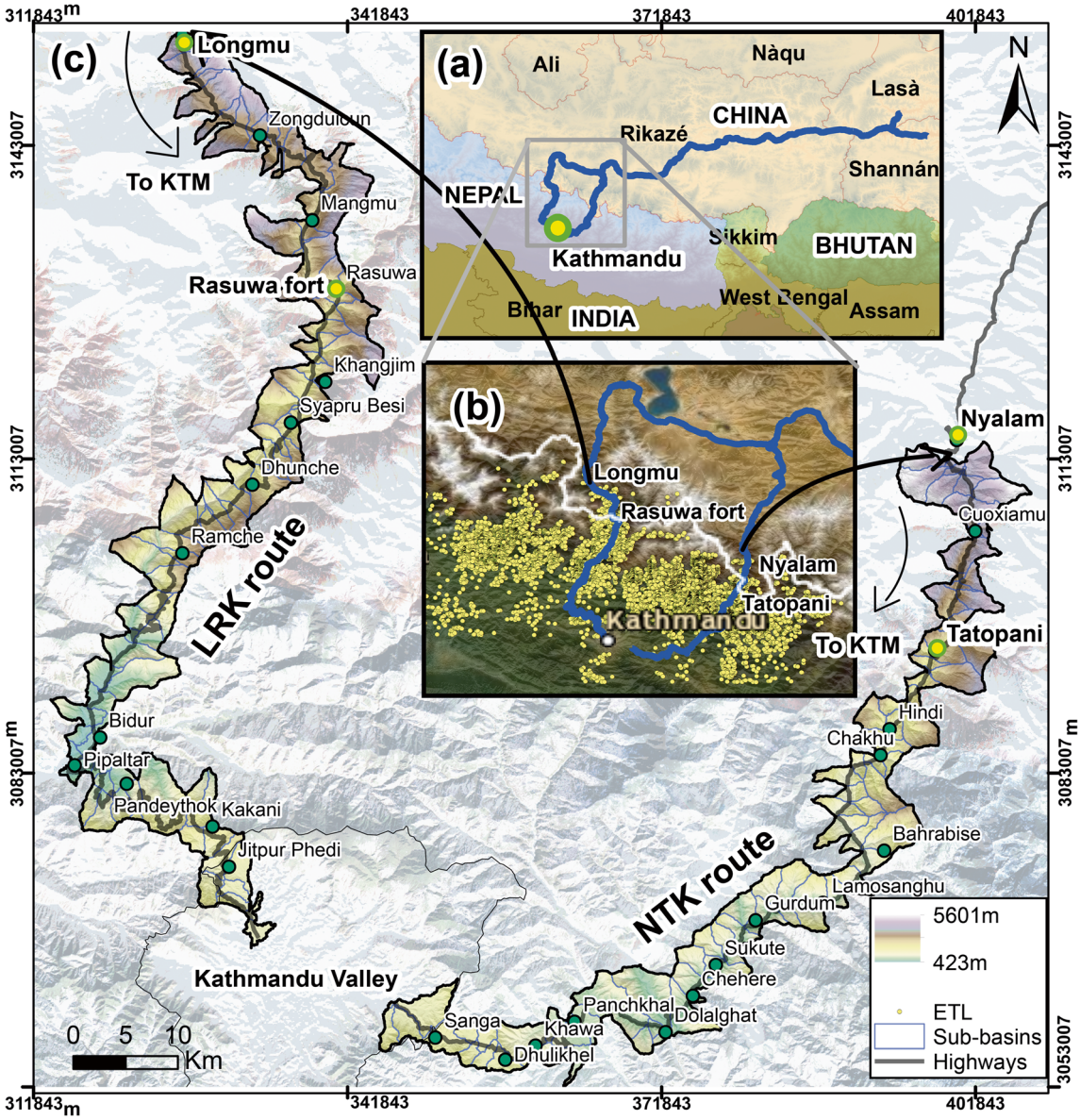

Fig. 1 The study area and road corridors. (a) LRK and NTK as strategic economic trade routes connecting China and Nepal. (b) Earthquake triggered landslides (ETL) distribution in the region from the 2015 Gorkha earthquake, data from (Gnyawali and Adhikari 2017). (c) Sub-basins along the river valleys of LRK and NTK as the area of analysis in this study

unusually high landslide hazard, mainly during the summer monsoons (Petley et al. 2007). Rivers incision into bedrock is at ~ 2–8 mm/year rate (Lavé and Avouac 2001). The annual average temperature varies from −6 to 22 degrees Celsius, and average rainfall varies from 31 to 201 mm.

(1) The Longmu–Rasuwa–Kathmandu (LRK) route is a 183 km section that descends from 3250 m above sea level (m a.s.l.) in Longmu, China to 450 m in Pipaltaar, Nepal, following the Trishuli river course and then further ascends to 1250 m in Kathmandu, Nepal. This route has strategic dual purposes: 1) transportation corridor and 2) the geo-spatial linking of China to India overland through Nepal (Beazley and Lassoie 2017). This route is now under prioritization for development because of three key reasons: 1) possibility of construction of dry ports at the border area, 2) planned extension of the Chinese railway line to the Nepal border and 3) it is the shortest route to India for trade exchange (Beazley and Lassoie 2017; Rana and Karmacharya 2016). Geologically, it intersects metamorphic and carbonate rocks (Wandrey and Law 1998). LRK has 90 sub-basins of streams draining primarily into the Trishuli River with a total area of 544 km^2.

(2) The Nyalam–Tatopani–Kathmandu (NTK) route is a 137 km section that descends from 3700 m a.s.l. in Nyalam, China to 575 m in Dolalghat of Nepal,

primarily following the Koshi river and then further ascends to 1250 m in Kathmandu, Nepal. NTK was recently closed due to heavy damage by the 2015 Gorkha earthquake and initiatives are now going on to reopen the route (Himalayan News Service 2018). Geologically, it intersects metamorphic and carbonate rocks along with mixed grain-sized and siliciclastic sedimentary rocks (Wandrey and Law 1998). NTK has 85 sub-basins of streams draining primarily into the Koshi river with a total area of 475.8 km^2.

The computation region is confined to stream catchments that intersect the highway and bounded by a 6 km buffer upslope. However, for the analysis region, a further reduced 2 km upslope buffer is applied and named the debris influence zone. These stream catchments intersecting the highway are the highway slope units because they overlap the slope units as defined by (Alvioli et al. 2016; Ba et al. 2018; Wang et al. 2017).

Datasets

Two sets of landslide inventory maps comprising all types of slope failures were prepared for this study: 1) rainfall triggered landslides (RTL) and 2) earthquake triggered landslides (ETL), Fig. 2.

(1) Rainfall-triggered landslides (RTL)

RTL were mapped by manually digitizing the bare earth-landslide scars in historical satellite images of Google Earth. It mainly consisted of CNES/Airbus, DigitalGlobe and SPOT imagery with resolution ranging from 1.5 to 2.5 m. Smaller area landslides tend to be erased from the landscape more quickly than larger area landslides due to vegetation cover. Thus, a multi-temporal inventory of 5 years was prepared. This included landslides from 2012 to 2015 (before the earthquake struck) and from 2016 to 2017 (after the earthquake). Partial imagery gaps at different time scales existed in some parts; however, a 5-year overall temporal coverage is assumed.

(2) Earthquake-triggered landslides (ETL)

The Mw 7.8, 2015 Gorkha earthquake struck the region on the 25th of April 2015. There were 553 aftershocks following the main shock (> 4.0 Mw) within the first 45 days (Adhikari et al. 2015), causing additional landslides. Thus, the ETL inventory comprised all landslides that were triggered by the main shock and subsequent aftershocks from 25th April to 15th June 2015. The inventory of (Roback et al. 2018) was clipped into the study region since it was comprehensive with the highest number of detected landslides in the study area among other published inventories. The ETL had been mapped by comparing pre- and post-event high-resolution DigitalGlobe, Worldview-2 and -3 satellite imagery, and supplemented with Astrium's Pleiades and Google Earth images in places of cloud-cover or distortion.

Determinants for landslides

Landslide determinants distribution along the LRK and NTK are shown in Figs. 3 and 4.

Slope

The slope determines the amount of runoff, distribution of groundwater and energy potential of the earth's soil erosion (Cooke and Doornkamp 1990). Surface runoff due to the force of gravity is accelerated on steeper slopes. In this study, the slopes were reclassified into eight equal classes l: 0–10°, 10–20°, ..., 60–70° and > 70°.

Aspect

Slope aspect is related to precipitation, natural vegetation thickness, wind impact, sunlight exposure and orientation of

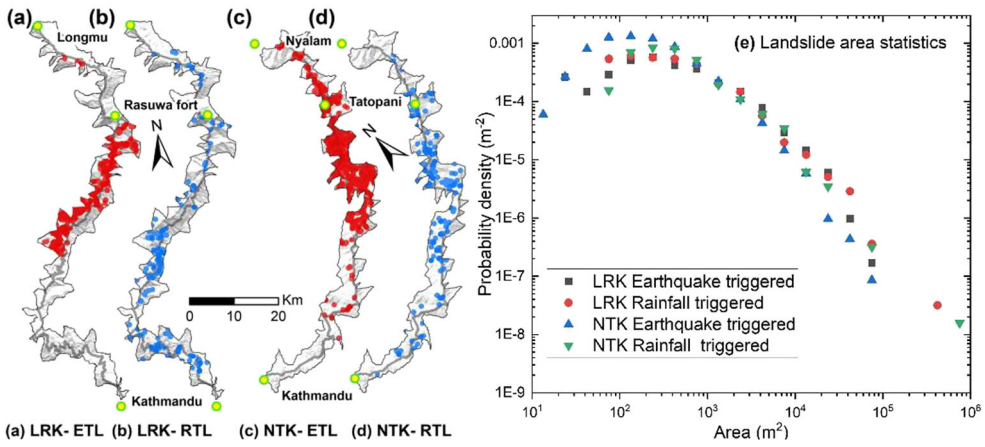

Fig. 2 Landslide inventories along the routes. (a) ETL along LRK. (b) RTL along LRK. (c) ETL along NTK. (d) RTL along NTK. (e) Landslide area probability (normalized number of landslides per logarithmic bin width and the total number of landslides) distribution along the routes

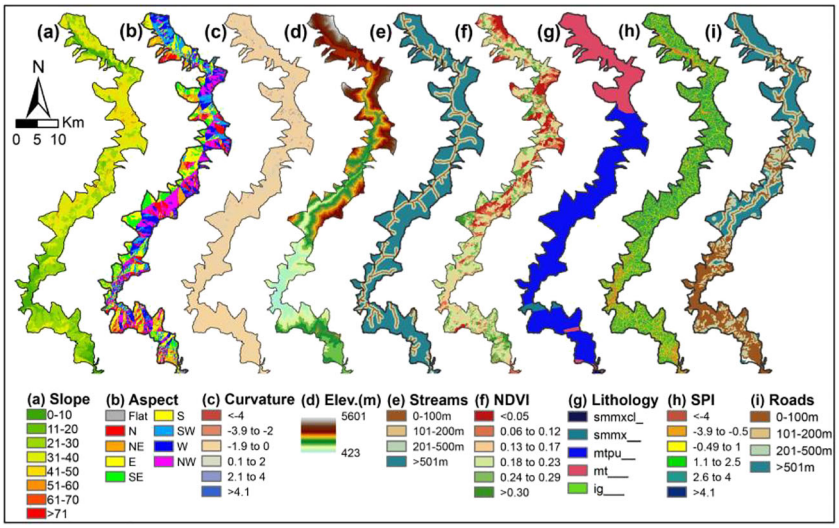

Fig. 3 Landslide determinants along the Longmu–Rasuwa–Kathmandu (LRK) route

discontinuities controlling the landslides (Ercanoglu et al. 2004) and in thecase of ETL, it is related to the direction of seismic energy release. The aspect was derived using the DEM and with the following eight common classes: N (337.5°–22.5°), NE (22.5°–67.5°), E, SE, S, SW, W and NW (292.5°–337.5°).

Curvature

Slope curvature controls the erosion process as it represents topographic morphology. The plan curvature indicates erosion and transport potential of slope material, while the profile curvature indicates the acceleration and deceleration of movement (Erener and Düzgün 2010). In this study, the total curvature is considered, which combines both. It is classified into six classes of equal intervals: < −4, −4 to −2, −2 to 0, 0 to 2, 2 to 4 and > 4. The negative curvature means concave surface, positive means convex and zero means flat ground.

Elevation

Both the road corridors descend sharply along the Himalayan river courses ranging from 423 to 5601 m a.s.l. in 183 km of LRK and 571 to 5601 m a.s.l. in 137 km of NTK. This large altitude variation is also reflected in changing precipitation zones, temperature, anthropogenic activities and the gravitational potential energy of landslides (Ercanoglu et al. 2004). Thus, altitude is chosen as a main parameter for this study. It is classified into equal intervals of 250 m.

Distance to streams

Riverbank erosion is another important cause of landslides (Zêzere et al. 1999). Slopes near streams are vulnerable to landsliding, due to bank cutting causing toe erosion or by water saturation reducing the frictional strength of the material. The streams distance was classified into four classes: 0–100 m, 100–200 m, 200–500 m and > 500 m.

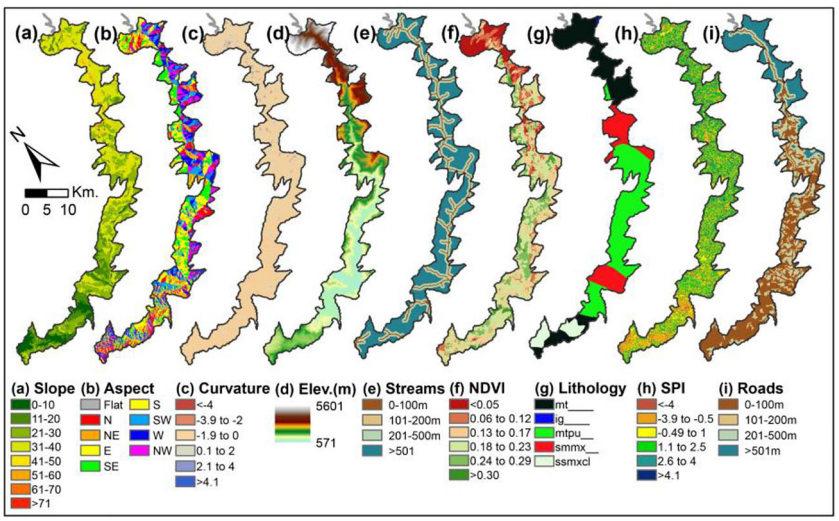

Fig. 4 Landslide determinants along the Nyalam–Tatopani–Kathmandu (NTK) route

Stream power index (SPI)

SPI is a measure of the erosive power of the stream. The SPI is defined as:

$$SPI = \log(A_s \times \tan\beta) \quad (1)$$

with A_s being the specific catchment area and β being the local slope, in degrees. SPI is divided into six classes based on natural breaks classification: < −4, −4 to −0.5, −0.5 to 1, 1 to 2.5, 2.5 to 4 and > 4.

Normalized vegetation difference index (NDVI)

NDVI indicates the presence, vigour and intensity of green vegetation in the study area (Erener and Düzgün 2010). It is calculated from a cloud-free Landsat 8 image, using the formula:

$$NDVI = \frac{(IR-R)}{(IR+R)} \quad (2)$$

where R and IR represent red and near-infrared bands of the electromagnetic spectrum.

Lithology

Lithology characterizes slope-forming material and affects the strength and permeability of slopes (Dai and Lee 2002). Four types of lithological covers are found in the study area: metamorphics (pure carbonate) (mtpu)-, metamorphics (mt), mixed sedimentary rocks with mixed grain size (smmx) and siliciclastic sedimentary rocks with mixed grain size and fossil plant organic material mentioned (smmxcl). At high altitudes, ice and glacier (ig) covers were also included in the lithological calculation.

Distance to roads

Roadside cut slopes and embankments are critical to landsliding in mountainous areas (Hearn and Shakya 2017). Multifold landslide occurrences are more observed near roadside slopes than on normal slopes in this region (McAdoo et al. 2018). Thus, distance to roads is an important factor here. It was categorized into four classes: 0–100 m, 100–200 m, 200–500 m and > 500 m.

Methods

A flowchart for the overall process adopted in this work is presented in Fig. 5.

Study area: slope units intersecting the highways

Hydrological regions bounded by drainage and ridge lines, also known as slope units, are reliable terrain mapping units for landslide susceptibility assessment (Alvioli et al. 2016; Guzzetti 2006). In this study, a 6 km buffer area around the highways and that enclosing the river valleys was chosen and a 12.5 m × 12.5 m digital elevation model (DEM) from ALOS Phased Array type L-band Synthetic Aperture Radar (PALSAR) was clipped in it. Sub-basins of drainage lines (min. contribution area = 3 km^2) were generated from this DEM using the ArcHydro tools in ArcGIS. Then, the sub-basins that intersected the roads were chosen as the mapping units. Some residual regions that cannot contribute slope debris on highways were clipped out manually. LRK had 90 such sub-basins and NTK had 85, Fig. 1. However, the final susceptibility maps are further clipped by a 2-km upslope buffer that encloses the maximum runout distance of all the mapped landslides.

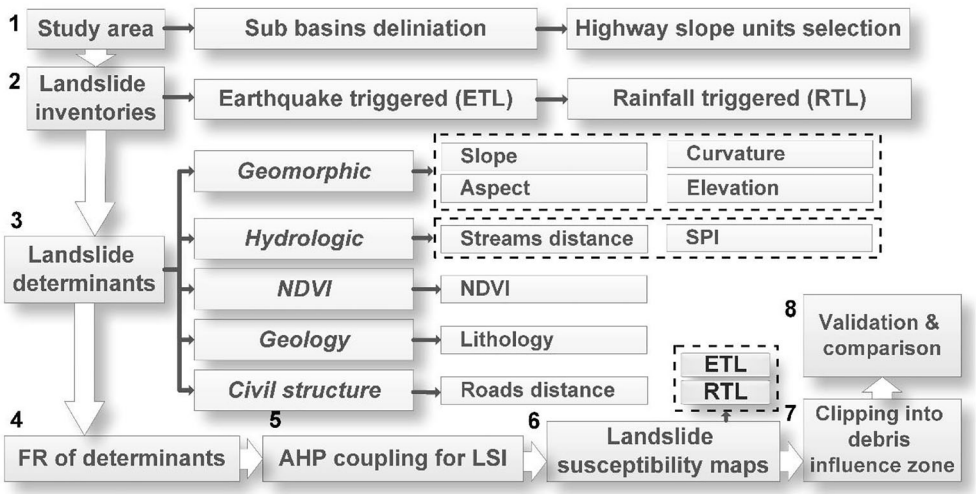

Fig. 5 Flowchart for mapping the landslide susceptibility

Landslide inventories and determinants

ETL polygons obtained from (Roback et al. 2018) were overlaid on Google earth and then RTL were mapped from 2012 to 2017. The ETL and RTL were split into two parts: 1) training set (~70% of the total landslides number) and 2) validation set (remaining ~30%), Fig. 2. This was done by random sampling and three independent and overlapping samples of training and validation sets were created for threefold cross validation. For example, in LRK route, 3 + 3 training and validation data for RTL and 3 + 3 for ETL were generated. The training landslides were used to train the susceptibility model. The geomorphic and hydrologic determinants were derived in GIS from the DEM. NDVI is calculated from the Landsat 8 image of 2015-01-24 with the least cloud cover. Lithological maps of Southeast Asia (Wandrey and Law 1998) in 1:10 miles were used for the geological determinant. Open street maps data was used for roads.

FR of determinants and AHP coupling

The landslide determinants were re-classified at suitable intervals as described above. Each sub-class of a determinant had a different impact on the landslide occurrence. Therefore, a rating of each subclass within each landslide determinant was done based on the landslide relative frequency ratio (FR) defined as:

$$FR = \frac{LF}{CA} / \sum \frac{LF}{CA} \tag{3}$$

where LF is the landslide number frequency recorded into the individual class and CA is the proportional class area. Then this value was normalized by the sum and named normalized frequency ratio (nFR). The larger value of nFR means that the parameter class is more dominant for landslide susceptibility. In this way, we get the individual impact of each subclass of the landslide determinant. Then, the next step was to couple it with the analytical hierarchy process (AHP) to quantify the relative weight of each of the nine landslide determinants.

Firstly, the number-weighted average FR is computed for each landslide determinant. Then pairwise comparisons are made based on these values for each of the landslide determinants and for all possible combinations. Finally, these values are fed into the pairwise comparison matrix. Once the comparison matrix is built, the mathematical processing of the AHP was implemented to calculate the susceptibility indices and followed by the generation of landslide susceptibility maps for ETL and RTL.

The AHP algorithm calculates the principal or maximum eigenvector of the comparison matrix yielding the proportional weights of each landslide determinant, which sum to 1. The consistency of the pairwise comparison matrix is described by the consistency ratio (CR), defined as the ratio of the random inconsistency index (RI) to the consistency index (CI), and is generally accepted when CR is <0.1 (Saaty 1980). The CI is expressed with Eq. 2:

$$CI = \frac{\lambda_{max} - n}{n - 1} \tag{4}$$

where λ_{max} is the major value of the comparison matrix and n is the order of the matrix. RI is the consistency of a randomly generated pairwise matrix, and it depends on the size of the matrix, Table 1 (Saaty 1980).

Calculation of landslide susceptibility

The normalized principal eigenvectors of each matrix, Tables 3 to 4, yield overall weight values for each landslide determinant by AHP, and for each class of a determinant, the weights were already determined by FR. The weights indicate the importance of the determinant and its class. Finally, the overall Landslide Susceptibility Index (LSI) is obtained by the weighted linear sum:

$$LSI = \sum_{j=1}^{n} W_j w_{ij} \tag{5}$$

where W_j is the weight value of landslide determinant j (from AHP), while w_{ij} is the weight value of class i of the determinant j (from FR), and n is the number of causative factors. The value of the LSI for each pixel gives the area of the LSI map.

Categorical classification of the LSI map is suitable for comparison studies; however, no common rules to categorize such continuous data is well established (Ayalew and Yamagishi 2005); different researchers use their own expert opinion to develop classes' boundaries (Kayastha et al. 2013). In this study, the desired landslide susceptibility maps were categorized into five susceptibility classes, defined by the natural breaks classification method (Demir et al. 2013). Finally, the LSI map was clipped into debris influence zones.

Validation of the susceptibility maps

In order to eliminate the performance measure variability arising from sampling variation, a threefold cross validation is adopted (Petschko et al. 2014). A single model performance is assessed through the prediction rate curve, which is a plot of cumulative percentage of observed validation landslides against the cumulative percentage of decreasing LSI values

Table 1 RI values based on the size of the matrix

n	1	2	3	4	5	6	7	8	9	10
RI	0.0	0.0	0.58	0.90	1.12	1.24	1.32	1.41	1.45	1.51

(Kayastha et al. 2013). This is done for all 12 dataset cases in ETL and RTL of the LRK and NTK. While extracting the LSI values, the majority cells value in the whole landslide body was chosen. The closer the AUC value is towards 100%, the more accurate the model.

Comparison of the two road corridors

For comparison between the two routes, the median value of LSI in each ETL and RTL was used to split high or low landslide probability for each pixel. Then, using the combine tool in GIS, each pixel was assigned either of these four values: (i) high ETL and RTL both, (ii) high ETL low RTL, (iii) high RTL low ETL or (iv) low ETL and RTL both. Then total area of each type of pixel was used for the route comparison.

Results

Landslide statistics

The total number of the ETL is higher than RTL, for both of the routes (LRK: 4 times, NTK: 13 times). The total number of ETL on NTK (2489nos.) is 3.4 times higher than LRK (727). The probability density of large area landslides is higher in the case of RTL, Fig. 2e. NTK has a higher number of smaller area (< 200 m^2) ETL, while LRK has higher number of larger area (larger than 10000 m^2) ETL, Fig. 2e. Further, the percentage of RTL within 100 m of the highways is higher than ETL in both the routes (Table 2). The landslide inventory and statistics are summarized in Table 2.

Spatial distribution and weights

A higher degree of spatial clustering is observed in ETL than RTL, Fig. 2. In the spatial analysis, slopes of 20 to 60 degrees, aspects of SE-S-SW and SPI >2.5 were susceptible in all four cases. Convex slopes (>2) were more susceptible in RTL. The elevation of 1750 to 2750 m a.s.l. was susceptible for ETL, while 500 to 3250 m a.s.l. was susceptible for RTL. NDVI range from 0.12 to 0.23 had peaks of nLF then dropped in RTL, while increasing NDVI values indicated an increase in nLF in ETL. In lithology, mtpu (metamorphic pure carbonate) and smmx (mixed sedimentary rocks with mixed grain size) were most susceptible in all cases. Stream distance <200 m had the highest nLF. Road distance <100 m had larger nLF (0.28 and 0.48) peaks in RTL, while that peak shifted to a higher distance of 200–500 m in ETL. The results of class weights of the data layers are shown in Fig. 6.

Pairwise comparison matrices for AHP is shown in Tables 3 and 4. In weight comparison of the determinants, elevation with average AHP weight (0.22), slope (0.20) and curvature (0.14) were important in ETL occurrences, whereas elevation with average AHP weight (0.24), aspect (0.16) and curvature (0.11) were important in the case of RTL. Lithology (0.05) and distance to roads (0.06) had the least influence in both cases. In the case of route-based comparison for LRK and NTK, the factor weights are similar. The results of the AHP factor weights are shown in the last column of Tables 3 and 4.

Landslide susceptibility maps

The landslide susceptibility maps for four cases: 1) LRK-ETL, 2) LRK-RTL, 3) NTK-ETL and 4) NTK-RTL are shown in Fig. 7. The proportion of high and very high classes of landslides susceptibility is higher in the LRK (125.25 km^2 in RTL, 75.17 km^2 in ETL) route than in the NTK (31.73 km^2 in RTL, 74.36 km^2 in ETL).

Validation

Table 5 shows the area under the curve (AUC) of prediction rate values for different random subsets of the training landslides in threefold validation. The variation of AUC is reasonably small in all cases. The maximum variation is observed in LRK ETL with 6.8% and minimum 0.8% in NTK ETL. Figure 8 shows the average prediction rate curves of threefold cross validation. On landslide type, ETL have higher prediction rates (85.5% LRK, 80.0% NTK) than RTL, while on roads, LRK has higher prediction rate (83% avg.) then NTK (77.6%).

Table 2 Landslide inventory statistics of LRK and NTK route

Types of landslides	Number of landslides				Average area ($\times 10^3 m^2$)		Percentage of landslides within 100 m of the highways	
	LRK		NTK		LRK	NTK	LRK	NTK
	Slope units	*Debris influence zone	Slope units	*Debris influence zone				
RTL	169	128	193	113	9.4	2532.0	47%	15%
ETL	727	336	2489	1085	5.9	2.6	36%	9%

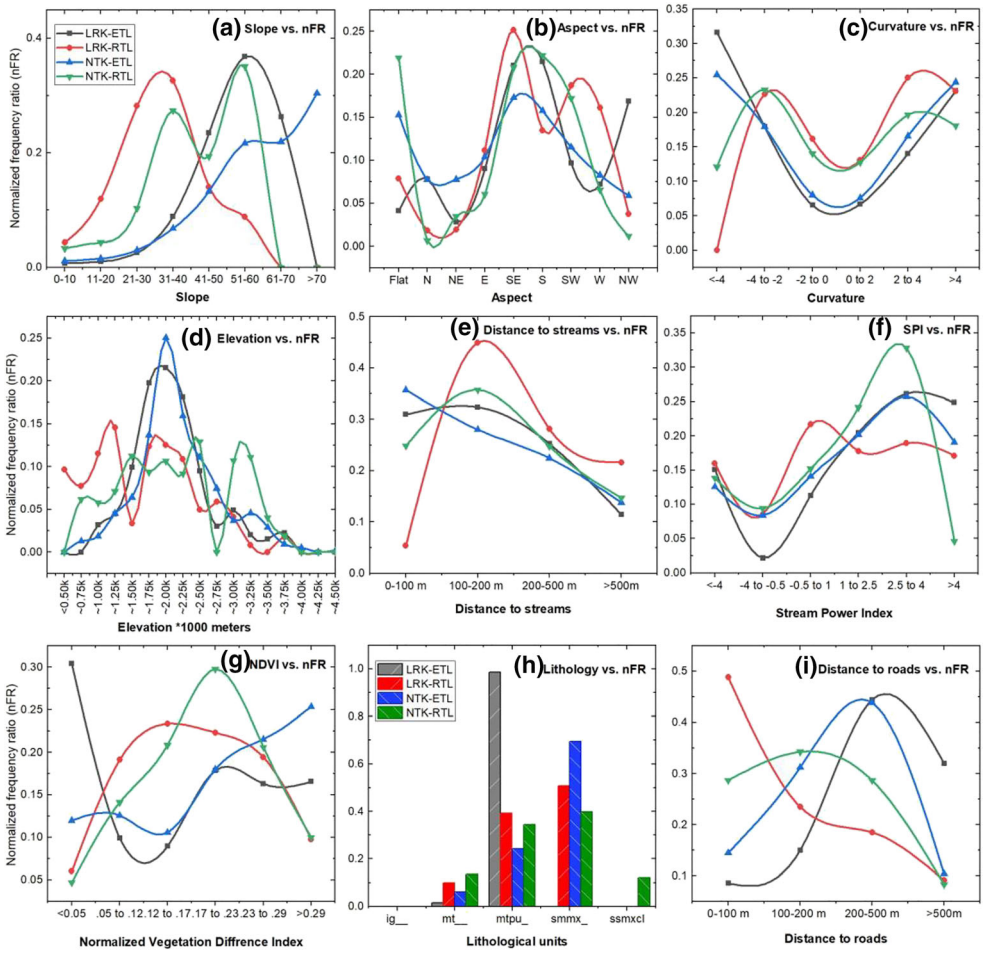

Fig. 6 Landslide determinants subclasses vs. normalized frequency ratio (nFR) plots

Route comparison

The NTK route is found safer in terms of landsliding in all cases, Fig. 9. For route comparison, the combined ETL and RTL susceptibility maps are useful, as shown in Fig. 10. NTK has 133.5 km^2 of high RTL or ETL (or both) landslide susceptible areas, whereas LRK has a 216.04 km^2 area as such.

Table 3 Pairwise comparison matrix for ETL and RTL of LRK route

Determinant	[1]		[2]		[3]		[4]		[5]		[6]		[7]		[8]		[9]		Eigen weight	
	ET	RT	ET	RT	ET	RT	ET	RT	ET	RT	ET	RT	ET	RT	ET	RT	ET	RT	ET	RT
[1] Slope	1.00	1.00																	0.17	0.08
[2] Aspect	0.62	1.88	1.00	1.00															0.11	0.15
[3] Curvature	0.88	1.38	1.42	0.73	1.00	1.00													0.15	0.11
[4] Elevation	1.38	3.23	2.23	1.72	1.57	2.35	1.00	1.00											0.24	0.26
[5] Streams	0.43	0.94	0.69	0.50	0.49	0.68	0.31	0.29	1.00	1.00									0.07	0.08
[6] SPI	0.45	1.23	0.73	0.65	0.52	0.89	0.33	0.38	1.06	1.31	1.00	1.00							0.08	0.10
[7] NDVI	0.47	1.19	0.75	0.63	0.53	0.86	0.34	0.37	1.09	1.27	1.03	0.96	1.00	1.00					0.08	0.10
[8] Lithology	0.18	0.71	0.29	0.38	0.20	0.52	0.13	0.22	0.42	0.76	0.40	0.58	0.39	0.60	1.00	1.00			0.03	0.06
[9] Roads	0.36	0.87	0.58	0.46	0.41	0.64	0.26	0.27	0.83	0.93	0.79	0.71	0.77	0.74	1.99	1.23	1.00	1.00	0.06	0.07

(Consistency ratio: ETL = 0.012, RTL = 0.052)

Table 4 Pairwise comparison matrix for ETL and RTL of NTK route

Determinant	[1]		[2]		[3]		[4]		[5]		[6]		[7]		[8]		[9]		Eigen weight	
	ET	RT	ET	RT	ET	RT	ET	RT	ET	RT	ET	RT	ET	RT	ET	RT	ET	RT	ET	RT
[1] Slope	1.00	1.00																	0.23	0.11
[2] Aspect	0.51	1.43	1.00	1.00															0.12	0.16
[3] Curvature	0.57	1.00	1.12	0.70	1.00	1.00													0.13	0.11
[4] Elevation	0.87	2.04	1.68	1.43	1.51	2.05	1.00	1.00											0.20	0.23
[5] Streams	0.30	0.76	0.58	0.53	0.52	0.76	0.35	0.37	1.00	1.00									0.07	0.09
[6] SPI	0.33	0.77	0.63	0.54	0.57	0.78	0.38	0.38	1.09	1.02	1.00	1.00							0.07	0.09
[7] NDVI	0.35	0.74	0.68	0.52	0.61	0.74	0.40	0.36	1.16	0.97	1.07	0.95	1.00	1.00					0.08	0.08
[8] Lithology	0.22	0.54	0.43	0.37	0.38	0.54	0.25	0.26	0.73	0.71	0.67	0.69	0.63	0.73	1.00	1.00			0.05	0.06
[9] Roads	0.26	0.58	0.50	0.40	0.45	0.58	0.30	0.28	0.86	0.76	0.79	0.75	0.74	0.78	1.18	1.08	1.00	1.00	0.06	0.07

(Consistency ratio: ETL = 0.001, RTL = 0.001)

Discussions

Landslide statistics and clustering

The size of ETL are mainly dependent on the shaking duration and partly on the topographic steepness (Collins and Jibson 2015; Marc et al. 2016). The size distributions of ETL and RTL landslides found in the slope units of these highways are comparable as observed in (Marc et al. 2019) for the region. However, some very large area landslides were found in cases of RTL for both highways. Intense precipitation, road proximity and presence of anthropogenic activities apparently seem to have increased the chances of these large area RTL (Jaboyedoff et al. 2015; McAdoo et al. 2018). The 3.4 times

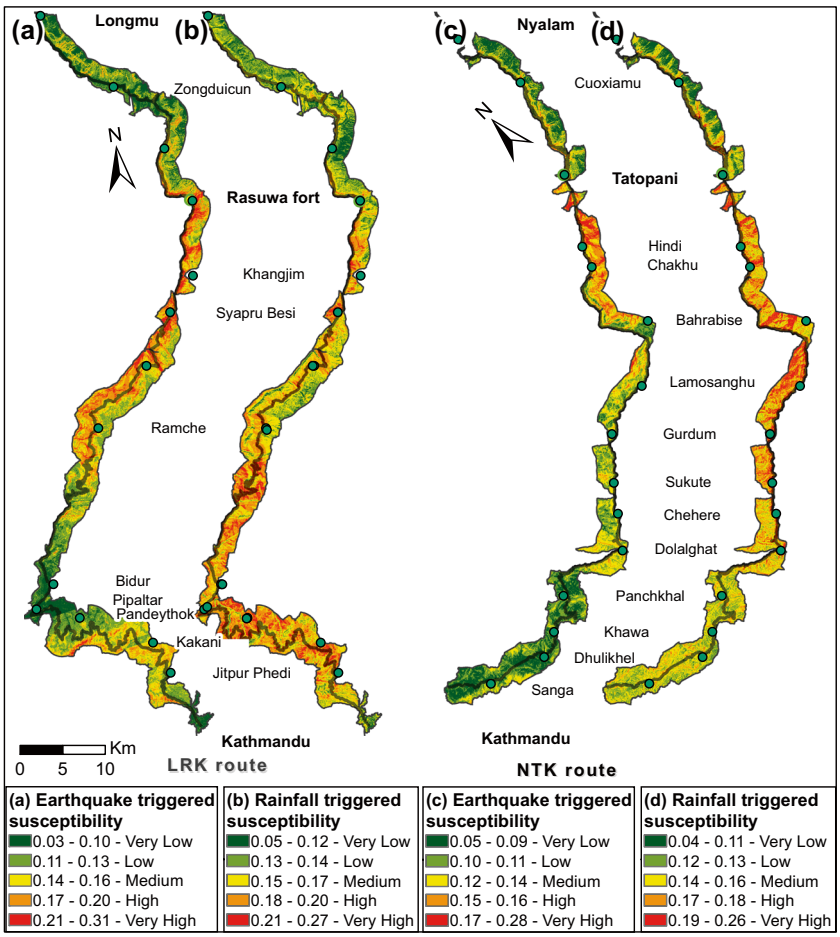

Fig. 7 Individual landslide susceptibility maps for the routes. (a) ETL along LRK. (b) RTL along LRK. (c) ETL along NTK. (d) RTL along NTK

Table 5 Results of threefold cross validation AUCs. V1, V2 and V3 are validation sets of landslides

Validation set	LRK				NTK			
	V1	V2	V3	Average	V1	V2	V3	Average
RTL	82.9%	80.5%	78.1%	80.5%	78.4%	73.5%	73.8%	75.3%
ETL	84.4%	82.6%	89.4%	85.5%	80.1%	79.3%	80.5%	80.0%

higher number of mapped ETL in NTK than LRK is because it passes near the end of a blind seismic rupture where maximum aftershock seismicity was observed (Adhikari et al. 2015).

RTL are found more uniformly distributed throughout the routes, Fig. 2b and d, while the spatial clustering of ETL is distinguishable in both the routes, Fig. 2a and c. The seismic energy of rupture from the 2015 Gorkha earthquake propagated in the eastwards direction from the epicentre (Mencin et al. 2016) (towards further west of LRK). Both these routes intersected the direction of energy propagation orthogonally, as they are north–south oriented. Thus, a clustering of the landslides in the portion parallel to that direction is consistent. The higher ETL density in part of the routes also correlates to high annual precipitation areas (Roback et al. 2018). Further, (Tsou et al. 2018) confirmed a similar clustering of the ETL on the Trishuli valley, on steeper slopes (> 35°) of fluvially incised V-shaped inner gorges de-buttressed and de-stabilized due to long-term river incision. The LRK passes primarily along this gorge, and our mapped landslides in RTL and ETL follow this trend, Fig. 6a.

Spatial distribution and weights analysis of determinants

In geomorphic determinants, RTL occurred on flatter slopes (31–40 degrees) than ETL (51–60 degrees), Fig. 6(a), because

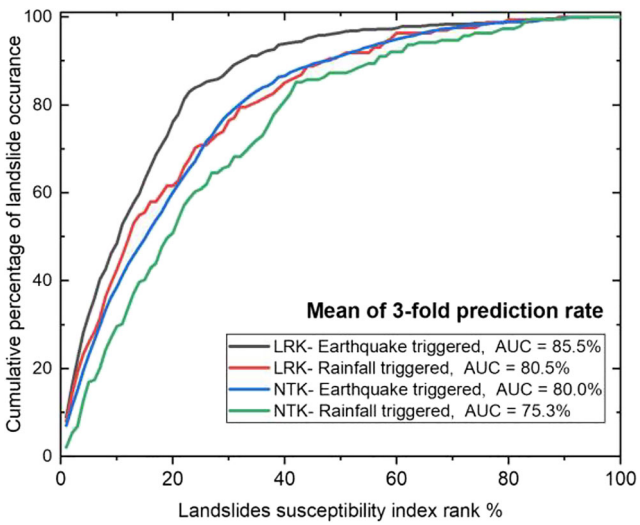

Fig. 8 Prediction rate curves for threefold cross validation where AUC represent the quality of the models used

RTL are mainly debris slides, flows or deep-seated failures that occurr on gentle slopes, while the ETL are mainly shallow disrupted slides or rockfalls on steeper slopes (Gnyawali and Adhikari 2017; Roback et al. 2018). In this respect, Fig. 6(b), the southward slopes (south–east, south and south–west) were susceptible in all four cases because the movement of monsoon moist airflow passes from the east and causes rainfall with an increase of elevation, especially on these windward slopes of the region (Zhang et al. 2018). Further, from satellite images, it is evident that the northern slopes are densely vegetated, while the southern slopes are barren and habitable, which make them more susceptible to landslides. In curvature, Fig. 6(c), convex slopes were more susceptible to RTL (values>2), while both convex and concave surfaces were equally susceptible to ETL. The elevation from 1750 m a.s.l. to 2750 m a.s.l., where maximum ETL was observed along both the routes, could be related to the elevation of the blind fault triggering this earthquake (Zhang et al. 2018), Fig. 6(d). In RTL, this range was different, i.e. 500 m a.s.l. to 3250 m a.s.l. The elevations lower than 3250 m a.s.l. were susceptible to landslides in both cases because of the existence of human activities and fluvial erosion, which is evident from the satellite images.

In hydrologic determinants, long term river incision has caused de-buttressing and destabilizing of the rock masses causing many landslides in this region (Tsou et al. 2018). Large GLOFs have also triggered many landslides due to toe-erosion (Marc et al. 2018). In ETL, Fig. 6(e), the closest distance to the streams (0–100 m) having the highest nFR (0.3 and 0.35) is presumably because of two reasons 1) presence of critically stable slopes at riversides and 2) river valley amplification of seismic waves. On the other hand, the peak of RTL occurs at a higher distance of 100–200 because their average sizes are larger, and thus their centroid points are at a larger distance to the streams. A higher stream power index indicated higher erosion potential of materials and hence higher landslide susceptibility, in both LRK and NTK, Fig. 6(f).

In NDVI, Fig. 6(g), the RTL had a peak at 0.17 to 0.23 NDVI class in both the routes, and the nFR decreased on increasing the NDVI values then after. The reason is that the RTL are mainly debris slides or flows and the presence of green vegetation reinforces the soil through its roots, reduces the energy of surface runoff and percolation, and thereby increases the slope stability. In ETL, the susceptibility increases with the increasing NDVI values because the shallow mass

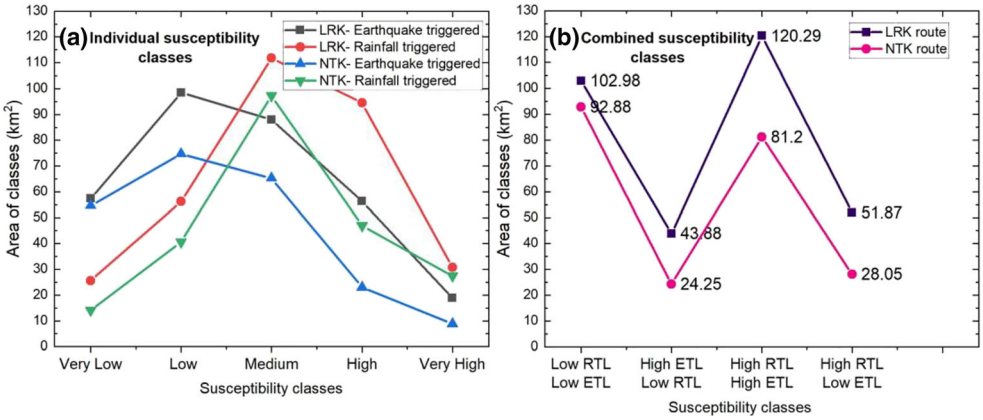

Fig. 9 Susceptibility comparison along the two routes. (a) Individual susceptibility comparison on ETL and RTL. (b) Combined susceptibility comparison based on the landslide type

disrupted slides or rockfalls in this category occurred on steep slopes that are devoid of vegetation cover. In lithology, Fig. 6 (h), there is not a significant relationship between the lithological units and the landslides distribution due to the Gorkha earthquake (Roback et al. 2018). The metamorphic-pure carbonate rocks (mtpu_) and mixed sedimentary rocks with mixed grain sizes (smmx_) were the most susceptible classes for both ETL and RTL. In civil structure, i.e. distance to road, Fig. 6(i), the road construction in this region often continues without due consideration of engineering geology (Dahal et al. 2010) leading to multi-fold increases in the landslide rates (McAdoo et al. 2018). The closest distance to roads (0–

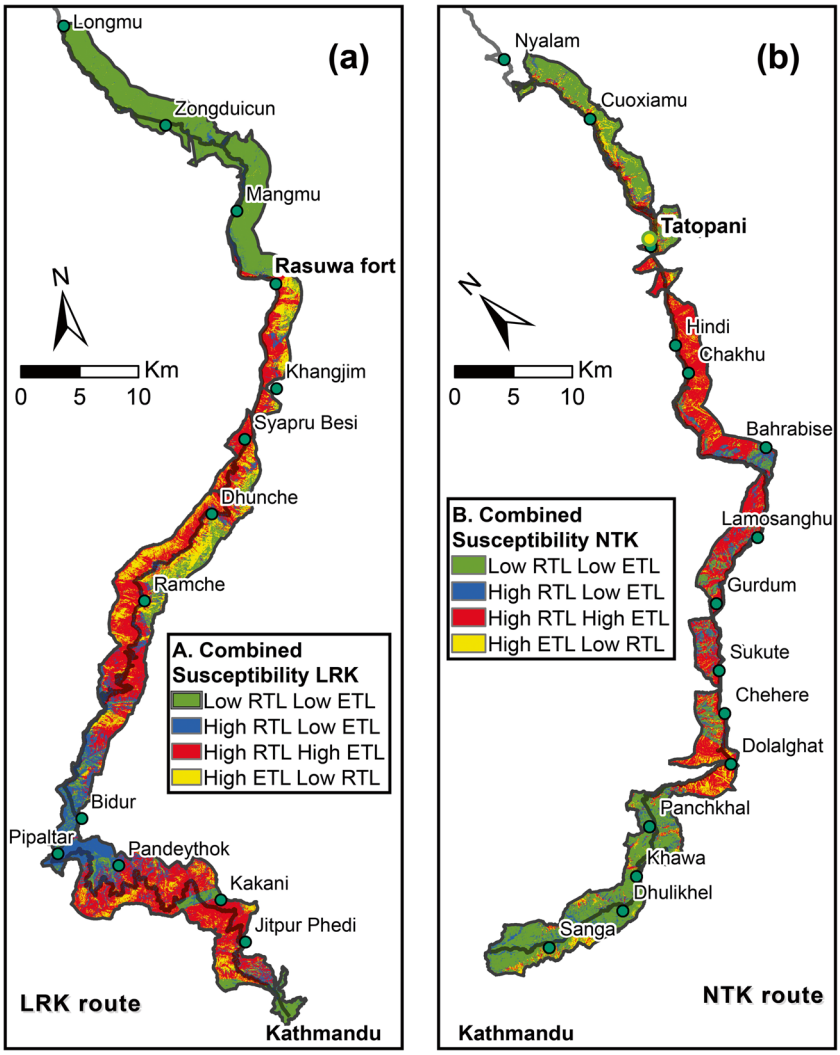

Fig. 10 Combined rainfall and earthquake triggered landslide susceptibility maps for the two routes

100 m) had larger nFR (0.28 and 0.48) in RTL; while in ETL, the peaks occurred at a slightly larger distance, i.e. 200–500 m. The earthquake triggered landslides distribution is mainly controlled by the ground accelerations (Meunier et al. 2007) and modulated by the local terrain factors (Meunier et al. 2008). Thus, this overruling relationship of ETL to the road proximity is consistent.

In overall weight analysis, the primary topographic proxies' elevation, slope, aspect and curvature have mainly governed the landslides susceptibility in both the routes. The large variation in elevation range for both the routes primarily relates to variation in precipitation zones, which is high in the middle hills. (Gallen et al. 2015) found that in moist, high relief, tectonically active and regions with strong climatic history, the rocks have reduced strength because of rapid weathering and water saturated conditions nearer to the fault zones. This fact enhances the landslide occurrence, and thus the dominance of elevation in landslides distribution for this region is consistent. Sharp variations in elevation in longitudinal direction throughout the route traverse seem to have escalated this control.

Landslide susceptibility maps

The produced susceptibility maps for RTL and ETL were positively correlated in both the routes (i.e. NTK = 0.66 and LRK = 0.18), Fig. 7. This means, for the NTK route, the RTL susceptibility map can describe 66% of ETL susceptibility areas and vice versa. However, for the LRK route, the ETL and RTL susceptibility areas are very different and describe only 18% of the area. It is important to note that the dynamic inter-dependence of the landslide determinants with the earthquake ground motion is not considered in this study. The use of RTL susceptibility maps is appropriate, but one should be careful in using the ETL susceptibility maps (Zhang et al. 2018) because it is subjected to change if a different nature of earthquake occurs.

For large scale planning and route comparisons, considering the unavailability of data for many earthquakes in the region, a simple combination strategy using the median value to separate high and low landslide occurrence probability is chosen. However, this threshold can be case dependent and might need more rigorous analysis. Further, their use should be done with proper care as they have varying model accuracy and thus more advanced methods of merging can be done in the future considering their inter-dependence.

Validation

For statistical validation, Fig. 8, AUCs in threefold prediction rate curves were satisfactory, e.g. LRK-ETL 85.5%, LRK-RTL 80.5%, NTK-ETL 80.0% and NTK-RTL 75.3% in success rate. Further, visual inspection of the susceptibility maps by overlaying the landslide polygons was done and found to be consistent for both large and small landslides. On checking, some large area landslides, e.g. Mankha rock avalanche in the NTK, Ramche landslide complex in the LRK, etc., lie in high and very high susceptibility classes. This also provides evidence of correctness in the modes used. In threefold validation, the minimum variation of AUC values observed in NTK ETL can be inferred to the larger number of observed and training ETL landslide samples in NTK (2489 nos.) compared to LKR (727), which had the highest variation.

From the AUC comparisons, we observe that the prediction performance of this coupled FR-AHP model is higher in the case of ETL than RTL. This finding infers that sufficiently complete inventories lead to better model training and predictability. This is because the ETL are triggered in a short time frame (one and half months, in this case) and most of the landslides had been mapped from the satellite images (Roback et al. 2018). On the other hand, the rainfall triggered landslides occurred in multiple events over a long period of time, and imagery gaps limited their complete mapping. Thus, this coupled FR-AHP method can produce better results when the event landslide inventories are sufficiently complete.

Route comparison

Although the number of mapped ETL in the NTK (1085 nos.) is larger than LRK (336 nos.), the geomorphological susceptibility of the slopes in the LRK was found more susceptible to landsliding. The observed higher number of landslides in the NTK is possibly because the seismic energy of rupture of the 2015 Gorkha earthquake propagated in the eastwards direction from the epicentre (Mencin et al. 2016), where the route crosses. Further, in the case of the RTL, the susceptibility is consistent with a high number of landslides observed within the debris influence zone.

In combined landslides susceptibility, the LRK has 1.6 times higher area of high RTL or ETL (or both types of landslides susceptibility classes) than NTK, Fig. 9(b). However, this LRK route is now under prioritization for its development considering the feasibility of dry port construction, railway extension and shorter route to reach India (Beazley and Lassoie 2017; Rana and Karmacharya 2016). Our findings suggest that it is likely to face higher mitigation and debris maintenance cost in the long run than the NTK route.

Conclusions

In this study, the earthquake and rainfall triggered landslides susceptibility assessment of two trans-Himalayan roads was conducted using the coupled FR-AHP method considering nine landslide determinants and by constricting the mapping

extent to the highway slope units. The conclusions can be summarized as follows:

- Landslides susceptibility is higher in the LRK route than NTK. Further attention has to be paid to landslides mitigation measures for LRK on prioritizing the route for high vehicle mobility in future. Elevation, slope angle and aspect mainly control landslides distribution in these north–south aligned Himalayan highways.
- For long route river valley corridors, constricting the study area within the highway slope units can also yield reasonable AUC for landslides susceptibility mapping. This approach can save considerable mapping and computation efforts and can further be extended in other computational extensive methods.
- The ETL and RTL susceptible areas are positively correlated. However, their degree of correlation can vary highly depending on the region. Thus, comprehensive landslide hazard assessments considering both types of landslides are a must.
- The AUCs for ETL (avg. 82.75%) were higher than that for RTL (avg. 77.9%) based on threefold validation prediction rate suggesting that the coupled FR-AHP method can produce better results when the event landslide inventories are sufficiently complete (which was in the case of ETL here). However, the RTL susceptibility maps can be reliable in detecting landslide prone areas, but for the ETL, more advanced methods considering earthquake scenarios are recommended to achieve sufficient reliability in them.

Acknowledgements This study was financially supported by the National Natural Science Foundation of China (No. 41661144039) and the Key Project of National Social and Scientific Fund Program (No. 16ZDA047).

Data availability The raw data required in this study are available upon request by contacting K. R. Gnyawali (gnyawalikr@hri.org.np).

Compliance with ethical standards

Conflict of interest The authors declare no conflict of interest.

References

Adhikari L, Gautam U, Koirala B et al (2015) The aftershock sequence of the 2015 April 25 Gorkha–Nepal earthquake. Geophys J Int 203: 2119–2124

Alvioli M, Marchesini I, Reichenbach P et al (2016) Automatic delineation of geomorphological slope units with r.slopeunits v1.0 and their optimization for landslide susceptibility modeling. Geosci Model Dev 9:3975–3991

Ayalew L, Yamagishi H (2005) The application of GIS-based logistic regression for landslide susceptibility mapping in the Kakuda-Yahiko Mountains, Central Japan. Geomorphology 65:15–31

Ba Q, Chen Y, Deng S et al (2018) A comparison of slope units and grid cells as mapping units for landslide susceptibility assessment. Earth Sci Inf 11:373–388

Bai S, Cheng C, Wang J et al (2013) Regional scale rainfall- and earthquake-triggered landslide susceptibility assessment in Wudu County, China. J Mt Sci 10:743–753

Beazley RE, Lassoie JP (2017) The future of himalayan mobilities. In: Beazley RE, Lassoie JP (eds) Himalayan mobilities: an exploration of the impact of expanding rural road networks on social and ecological systems in the Nepalese Himalaya. Springer, Cham, pp 125–160

Camilo DC, Lombardo L, Mai PM et al (2017) Handling high predictor dimensionality in slope-unit-based landslide susceptibility models through LASSO-penalized generalized linear model. Environ Model Softw 97:145–156

Collins, BD, Jibson RW (2015) Assessment of existing and potential landslide hazards resulting from the April 25, 2015 Gorkha, Nepal earthquake sequence (ver. 1.1, August 2015). US Geological Survey Open-File Report 2015 1142:50

Cooke R, Doornkamp JC (1990) Geomorphology in environmental management: a new introduction. Oxford University Press, New York

Corominas J, van Westen C, Frattini P et al (2013) Recommendations for the quantitative analysis of landslide risk. Bull Eng Geol Environ 73: 209

Dahal RK, Hasegawa S (2008) Representative rainfall thresholds for landslides in the Nepal Himalaya. Geomorphology 100:429–443

Dahal RK, Hasegawa S, Bhandary N et al (2010) Low-cost road for the development of Nepal and its engineering geological consequences. Geologically Active, Proceedings of the 11th IAEG Congress, pp 4085–4094

Dai FC, Lee CF (2002) Landslide characteristics and slope instability modeling using GIS, Lantau Island, Hong Kong. Geomorphology 42:213–228

Demir G, Aytekin M, Akgün A et al (2013) A comparison of landslide susceptibility mapping of the eastern part of the north Anatolian fault zone (Turkey) by likelihood-frequency ratio and analytic hierarchy process methods. Nat Hazards 65:1481–1506

Dongtao M, Jianjun T, Peng C, Ruren L (2004) Approach to mountain hazards in Tibet, China. J Mt Sci 1:143–154

Ercanoglu M, Gokceoglu C, Van Asch TWJ (2004) Landslide susceptibility zoning of north of Yenice (NW Turkey) by multivariate statistical techniques. Nat Hazards 32:1–23

Erener A, Düzgün HSB (2010) Improvement of statistical landslide susceptibility mapping by using spatial and global regression methods in the case of more and Romsdal (Norway). Landslides 7:55–68

Fell R, Corominas J, Bonnard C et al (2008) Guidelines for landslide susceptibility, hazard and risk zoning for land use planning. Eng Geol 102:85–98

Gallen SF, Clark MK, Godt JW (2015) Coseismic landslides reveal near-surface rock strength in a high-relief, tectonically active setting. Geology 43:11–14

Gnyawali KR, Adhikari BR (2017) Spatial relations of earthquake induced landslides triggered by 2015 Gorkha earthquake mw = 7.8. In: advancing culture of living with landslides. Springer , Cham, pp 85–93

Goda K, Kiyota T, Pokhrel RM et al (2015) The 2015 Gorkha Nepal earthquake: insights from earthquake damage survey. Front Built Environ 1:1–15

Guzzetti F (2006) Landslide hazard and risk assessment. PhD Thesis, University of Bonn

Guzzetti F, Reichenbach P, Cardinali M et al (2005) Probabilistic landslide hazard assessment at the basin scale. Geomorphology 72:272–299

Hashash Y, Tiwari B, Moss RE et al (2015) Geotechnical field reconnaissance: Gorkha (Nepal) earthquake of April 25 2015 and related

shaking sequence. GEER Association Report No. GEER-040, pp 1–250

Hearn GJ, Shakya NM (2017) Engineering challenges for sustainable road access in the Himalayas. Q J Eng Geol Hydrogeol 50:69–80

Himalayan News Service (2018) Tatopani border point likely to reopen soon. The Himalayan Times, Kavre

Jaboyedoff M, Leibundgut G, Penna I, et al (2015) Characterization of the jure (Sindhupalchok, Nepal) landslide by TLS and field investigations. EGU General Assembly Conference Abstracts

Kayastha P, Dhital MR, De Smedt F (2013) Application of the analytical hierarchy process (AHP) for landslide susceptibility mapping: a case study from the Tinau watershed, West Nepal. Comput Geosci 52: 398–408

Lavé J, Avouac JP (2000) Active folding of fluvial terraces across the Siwaliks Hills, Himalayas of Central Nepal. J Geophys Res: Solid Earth 105:5735–5770

Lavé J, Avouac JP (2001) Fluvial incision and tectonic uplift across the Himalayas of Central Nepal. J Geophys Res: Solid Earth 106: 26561–26591

Li Y, Chen G, Tang C et al (2012) Rainfall and earthquake-induced landslide susceptibility assessment using GIS and artificial neural network. Nat Hazards Earth Syst Sci 12:2719–2729

Lombardo L, Mai PM (2018) Presenting logistic regression-based landslide susceptibility results. Eng Geol 244:14–24

Marc O, Behling R, Andermann C et al (2019) Long-term erosion of the Nepal Himalayas by bedrock landsliding: the role of monsoons, earthquakes and giant landslides. Earth Surf Dynam 7:107–128

Marc O, Hovius N, Meunier P et al (2016) A seismologically consistent expression for the total area and volume of earthquake-triggered landsliding. J Geophys Res: Earth Surf 121:640–663

McAdoo BG, Quak M, Gnyawali KR et al (2018) Roads and landslides in Nepal: how development affects environmental risk. Nat Hazards Earth Syst Sci 18:3203–3210

Mencin D, Bendick R, Upreti BN et al (2016) Himalayan strain reservoir inferred from limited afterslip following the Gorkha earthquake. Nat Geosci 9:533–537

Meunier P, Hovius N, Haines AJ (2007) Regional patterns of earthquake-triggered landslides and their relation to ground motion. Geophys Res Lett. https://doi.org/10.1029/2007gl031337

Meunier P, Hovius N, Haines JA (2008) Topographic site effects and the location of earthquake induced landslides. Earth Planet Sci Lett 275: 221–232

Mugnier J-L, Jouanne F, Bhattarai R et al (2017) Segmentation of the Himalayan megathrust around the Gorkha earthquake (25 April 2015) in Nepal. J Asian Earth Sci 141:236–252

Myronidis D, Papageorgiou C, Theophanous S (2016) Landslide susceptibility mapping based on landslide history and analytic hierarchy process (AHP). Nat Hazards 81:245–263

Petley DN, Hearn GJ, Hart A et al (2007) Trends in landslide occurrence in Nepal. Nat Hazards 43:23–44

Petschko H, Brenning A, Bell R et al (2014) Assessing the quality of landslide susceptibility maps – case study Lower Austria. Nat Hazards Earth Syst Sci 14:95–118

Pradhan AMS, Kim YT (2016) Evaluation of a combined spatial multi-criteria evaluation model and deterministic model for landslide susceptibility mapping. CATENA 140:125–139

Rana PB, Karmacharya B (2016) Nepal: a connectivity-driven development strategy. Connecting asia-infrastructure for integrating south and southeast asia. Edward, Cheltenham, pp 330–358

Roback K, Clark MK, West AJ et al (2018) The size, distribution, and mobility of landslides caused by the 2015 Mw7.8 Gorkha earthquake, Nepal. Geomorphology 301:121–138

Saaty TL (1980) The analytic hierarchy process. McGraw Hill, Pittsburgh

Saaty TL (2005) Theory and applications of the analytic network process: decision making with benefits, opportunities, costs, and risks. RWS, Pittsburgh

Saaty TL, Vargas LG (2001) Models, methods, concepts & applications of the analytic hierarchy process. Springer, New York

Tian Y, Xu C, Chen J, Hong H (2016) Spatial distribution and susceptibility analyses of pre-earthquake and coseismic landslides related to the Ms 6.5 earthquake of 2014 in Ludian, Yunan, China. Geocarto Int 32:978–989

Tsou C-Y, Chigira M, Higaki D et al (2018) Topographic and geologic controls on landslides induced by the 2015 Gorkha earthquake and its aftershocks: an example from the Trishuli Valley, Central Nepal. Landslides 15:953–965

Wandrey CJ, Law BE (1998) Geologic map of southasia (geo8ag). Central Energy Resources Team, United States Geological Survey, Denver

Wang F, Xu P, Wang C et al (2017) Application of a GIS-based slope unit method for landslide susceptibility mapping along the Longzi River, southeastern Tibetan plateau, China. ISPRS Int J Geo Inf 6:172

Xu C, Tian Y, Zhou B et al (2017) Landslide damage along Araniko highway and Pasang Lhamu highway and regional assessment of landslide hazard related to the Gorkha, Nepal earthquake of 25 April 2015. Geoenviron Disast 4:14

Zêzere JL, de Brum FA, Rodrigues ML (1999) The role of conditioning and triggering factors in the occurrence of landslides: a case study in the area north of Lisbon (Portugal). Geomorphology 30:133–146

Zhang J, van Westen CJ, Tanyas H, et al (2018) How size and trigger matter: analyzing rainfall- and earthquake-triggered landslide inventories and their causal relation in the Koshi River basin, central Himalaya. Nat Hazards Earth Syst Sci Discuss. https://doi.org/10.5194/nhess-2018-109